Capacity Analysis of NOMA With mmWave Massive MIMO Systems

Di Zhang, *Student Member, IEEE*, Zhenyu Zhou, *Member, IEEE*, Chen Xu, *Member, IEEE*, Yan Zhang, *Senior Member, IEEE*, Jonathan Rodriguez, *Senior Member, IEEE*, and Takuro Sato, *Fellow, IEEE*

***Abstract*— Non-orthogonal multiple access (NOMA), millimeter wave (mmWave), and massive multiple-input-multiple-output (MIMO) have been emerging as key technologies for fifth generation mobile communications. However, less studies have been done on combining the three technologies into the converged systems. In addition, how many capacity improvements can be achieved via this combination remains unclear. In this paper, we provide an in-depth capacity analysis for the integrated NOMA-mmWave-massive-MIMO systems. First, a simplified mmWave channel model is introduced by extending the uniform random single-path model with angle of arrival. Afterward, we divide the capacity analysis into the low signal to noise ratio (SNR) and high-SNR regimes based on the dominant factors of signal to interference plus noise ratio. In the noise-dominated low-SNR regime, the capacity analysis is derived by the deterministic equivalent method with the Stieltjes–Shannon transform. In contrast, the statistic and eigenvalue distribution tools are invoked for the capacity analysis in the interference-dominated high-SNR regime. The exact capacity expression and the low-complexity asymptotic capacity expression are derived based on the probability distribution function of the channel eigenvalue. Finally, simulation results validate the theoretical analysis and demonstrate that significant capacity improvements can be achieved by the integrated NOMA-mmWave-massive-MIMO systems.**

***Index Terms*— mmWave, NOMA, massive MIMO, capacity analysis, Stieltjes and Shannon transform, statistics and probability analysis.**

Manuscript received October 15, 2016; revised February 21, 2017; accepted March 12, 2017. This work was supported in part by the National Science Foundation of China under Grant 61601180 and Grant 61601181, in part by the Fundamental Research Funds for the Central Universities under Grant 2016MS17 and Grant 2017MS13, in part by the Beijing Natural Science Foundation under Grant 4174104, in part by the Beijing Outstanding Young Talent under Grant 2016000020124G081, and in part by the projects 240079/F20 funded by the Research Council of Norway. *(Corresponding author: Zhenyu Zhou.)*

D. Zhang is with the State Key Laboratory of Alternate Electrical Power System with Renewable Energy Sources, School of Electrical and Electronic Engineering, North China Electric Power University, Beijing 102206, China, and also with GITS/GITI, Waseda University, Tokyo 169-0072, Japan (e-mail: di_zhang@fuji.waseda.jp).

Z. Zhou and C. Xu are with the State Key Laboratory of Alternate Electrical Power System with Renewable Energy Sources, School of Electrical and Electronic Engineering, North China Electric Power University, Beijing 102206, China (e-mail: zhenyu_zhou@ncepu.edu.cn; chen.xu@ncepu.edu.cn).

Y. Zhang is with the Department of Informatics, University of Oslo, N-0373 Oslo, Norway, and also with the Simula Research Laboratory, Fornebu, Norway (e-mail: yanzhang@ieee.org).

J. Rodriguez is with the Institutõ de Telecomunicações, 3810-193 Aveiro, Portugal, and also with the University of South Wales, Pontypridd CF37 1DL, U.K. (e-mail: jonathan@av.it.pt).

T. Sato is with GITS/GITI, Waseda University, Tokyo 169-0072, Japan (email: t-sato@waseda.jp).

Digital Object Identifier 10.1109/JSAC.2017.2699059

I. Introduction

WITH even higher transmission rate claimed by the fifth generation (5G) wireless communications, spectrum efficiency (SE) [1]–[4] and energy efficiency (EE) [5], [6] are categorized as two main topics of the study. In which, millimeter wave (mmWave) [1], non-orthogonal multiple access (NOMA) [3], [4], and massive multi-input-multi-output (massive MIMO, also known as large-scale antenna system [7], large-scale MIMO [8]–[10]) [2] are noticed a lot both in academia and industry. MmWave refers to the frequency with 30 $\sim$ 300 GHz [11]. With shorter propagation distance and even higher frequency, the propagation characteristics are normally different from existing macro waves in use. In this regard, the propagation characteristics and channel model were intensively investigated at the incipient stage of mmWave studies [1], [12].

Other than the mmWave, NOMA was proposed to alleviate the spectrum bottleneck by invoking the superposition coding of multiple users in the same frequency, thereby, enhancing the systems' SE performance [13]. In NOMA studies, transmit power values amongst users are exploited to separate signals belonging to different users. Research topics such as beamforming design [14], user pairing [15], and power allocation [16], etc., were intensively investigated.

On the other hand, massive MIMO was introduced as well to tumble down the 5G's SE and EE requirement toughies [17]. The benefit of massive MIMO is that, with even larger antenna number, thermal noise and fast fading effects can be averaged out [2]. Besides the studies on SE issue, prior studies on massive MIMO's EE issue mostly focused on the effective engaged component selection method design, energy harvesting and content sharing technologies and their optimization methods, such as the work in [18]–[21].

A. Related Work

The related antecedent work is summarized as follows. For mmWave communications, the channel models were characterized and analyzed in [1], [12], and [22]. In [1], the angle of departure (AoD), angel of arrive (AoA), and channel gain characteristics of mmWave channels were estimated for both light of sight (LOS) and non light of sight (NLOS) paths to obtain a general channel model. In [12], a structured compressive sensing (SCS)-based channel estimation scheme was proposed. In which, the angular sparsity was employed as well to reduce the required pilot overhead. In [22], the mmWave channel was estimated with mmWave band (from 28 to 73 GHz) propagation characteristics. Besides, the cellular capacity was evaluated based on the experiment data collected from New York City. The simplified uniform random single-path (UR-SP) model was adopted for optimal beamforming design in mmWave communications [23]. Alkhateeb *et al.* [24], investigated the Kronecker channel model and proposed a hybrid pre-coding method for mmWave communications.

For the aspect of integrating NOMA with massive MIMO, a joint antenna selection and user scheduling algorithm was proposed in [25]. Numerical results showed that the proposed algorithm achieved better search efficiency in single-band two-user scenario. The simplified and limited feedback scenario for NOMA-MIMO systems was studied in [26]; where the NOMA-MIMO channel was decomposed into multiple NOMA-SISO channels. In the study of [27], the outage probability was investigated for NOMA-massive-MIMO systems. To integrate the massive MIMO with mmWave, the majority prior work focused on the beamforming design. For example, an interference-aware (IA) beam selection scheme was proposed by [28]; it can achieve near-optimal sum rate with better EE performance compared with conventional schemes. However, fewer studies have been done on NOMA-mmWave or on the integration of mmWave, NOMA and massive MIMO. From an intuitionistic perspective, by integrating these three, better SE and sum rate performances can be obtained. However, by what scale this increment can be is still ambiguous.

For the capacity analysis, various studies have been done before. For instance, the reservation-based random access wireless network capacity was investigated in [29] with addressed upper and lower bound expressions. Recently, the random matrix theory (RMT) tools are intensively noticed and have been vastly used to tame the performance of massive MIMO systems. The majority work of this focused on the closed-form expressions for critical parameter analysis, such as the ergodic capacity, higher-order capacity moments, and outage probability [27], [30]–[36]. Among the various mathematical tools provided by RMT, the deterministic equivalent method was introduced by [30], [31], [37], and [38]. In which, the Stieltjes-Shannon transform method [30]–[32], Gaussian method [34], and free probability theory [33] play critical roles. On the other hand, the statistics and probability analysis method was widely applied for capacity [35] and outage probability analysis [27] in massive MIMO systems. But still, for the more complicated NOMA-mmWave-massive-MIMO systems, these methods cannot be adopted directly, especially with the NOMA decoding scheme. Low-complexity asymptotic method is of great importance in this case.

B. Contributions

The aforementioned work plays vital role and lies solid foundation for the study of mmWave, NOMA and massive MIMO. In this paper, we step further to study the integrated NOMA-mmWave-massive-MIMO systems and provide a theoretical analysis on the achievable capacity. The main contributions of this paper are summarized as follows:

- The model of the integrated NOMA-mmWave-massive-MIMO systems is systematically introduced. To settle down the intractable characteristics with mmWave channel, a simplified mmWave channel model is introduced by extending the UR-SP model with AoA.
- For the capacity analysis, it is divided into the low signal to noise ratio (SNR) and high-SNR regimes to simplify the analysis. In the noise-dominated low-SNR regime, the capacity analysis is derived by the deterministic equivalent method with the Stieltjes-Shannon transform. During the analytical process, we provide mathematical proofs for the relationship between the Stieltjes transform and the Shannon transform. In the interference-dominated high-SNR regime, the deterministic equivalent method is no longer valid. In this regard, the exact capacity expression as well as a low-complexity special case (the numbers of paths, antennas, and user terminals are equal) expression are derived with the statistic and eigenvalue distribution tools.
- We evaluate the derived capacity expressions under both low-SNR and high-SNR regimes, and investigate the impacts of the numbers of LOS paths, antennas, and user terminals on the system performance. In the low-SNR regime, it is found that SNR and user number have positive correlations with the systems' capacity performance. This significantly outperforms the existing long term evolution (LTE) systems especially under the cell-edge scenario. In the high-SNR regime, numerical results manifest the matching relationship between the asymptotic PDF expression and the exact PDF expression. In addition, we find that the number of LOS paths has positive but ignorable effect to the capacity increment.

C. Organizations

The rest of this paper is organized as follows. The systems' model as well as the channel model are introduced by section II. The capacity analysis in the low-SNR regime is investigated by section III. Afterwards, section IV provides the capacity analysis for the high-SNR regime. The numerical results are given in section V. The main results and discussions are provided by section VI. All of the mathematical proofs are given by the Appendices.

D. Notations

Throughout the paper, the uppercase boldface letters, lowercase boldface letters, and normal letters are used to represent the matrix, vector, and scalar quantity, respectively. Furthermore, $\mathbb{C}$ and $\mathbb{R}$ denote the sets of complex and real numbers, respectively. $\mathbf{A}^H$ denotes the Hermitian transposition of a matrix $\mathbf{A}$. $\mathbf{A}_{i,j}$ is the (i, j)-th entry of a matrix $\mathbf{A}$ with the i-th row and j-th column. Additionally, $tr(\mathbf{A})$, $\det(\mathbf{A})$, and $\mathbb{E}(\mathbf{A})$ denote the trace, determinant, and expectation of the matrix $\mathbf{A}$, respectively. Moreover, $\mathbf{A}^{-1}$ is the inverse transpose of matrix $\mathbf{A}$. Finally, inf and sup are used to denote the infimum and supremum.

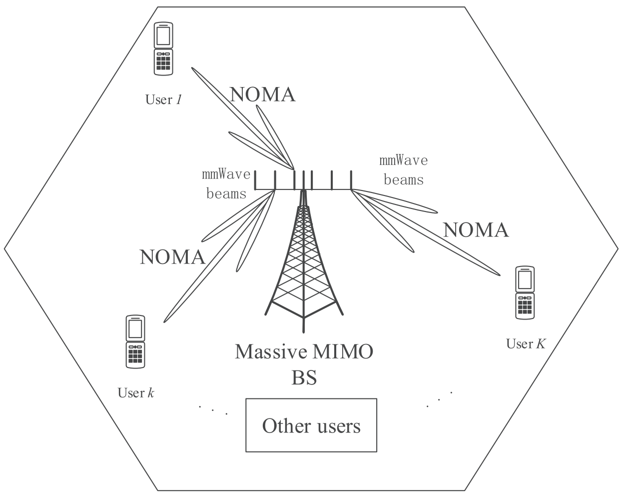

Fig. 1. The conceptual model of the NOMA-mmWave-massive-MIMO systems.

II. SYSTEM MODEL

In this section, firstly, the NOMA-mmWave-massive-MIMO systems model in the downlink is elaborated. We further propose a simplified mmWave channel model by extending the UR-SP model with AoA and express it in matrix form.

A. The NOMA-mmWave-Massive-MIMO Systems' Model

The NOMA-mmWave-massive-MIMO systems' model in the downlink that focused by this study is shown in Fig. 1. It consists of a massive MIMO BS that serving less but multiple user terminals (with number K). As shown here, the transmission is carried out in the mmWave frequency with mmWave beams. In addition, within each beam, the NOMA encoding scheme is utilized to encode the transmit signal.

With NOMA encoding scheme, the same spectrum resource block [13] is shared by multiple users within the same user group (it is assumed that the NOMA users within each frequency resource block is one user group). Among different user groups, orthogonal frequency correlations are assumed to isolate the inter-channel interference. The optimal power allocation problem of NOMA-MIMO has been investigated by prior studies [15], [39]. In this paper, we focus on the capacity analysis of the proposed NOMA-mmWave-massive-MIMO systems by assuming that power value is different amongst different users with regards to the NOMA concept [27]. This is due to the fact that the optimal power allocation study based on the scenario that the transmission rate requirement of each user is given beforehand [15], [39]. In addition, this capacity expression can also be applied for the optimal power allocation scenario while giving the transmission rate requirement of each user and the component carrier (CC) bandwidth. The optimal power allocation study can be done in future based on the NOMA-mmWave-massive-MIMO system s' model. At the receiver side, user can make use of SIC [27], [40] to remove the interferences from other users with higher orders. The remaining information from low order users is treated as interference.[1] With perfect orthogonal characteristics among channels of different user groups, the inter-channel interference caused by users in different groups can be ignored. Thus co-channel interference is mainly from users in the same group with a lower order.

With mmWave frequency in hand, much wider bandwidth can be allocated compared with macro wave frequency used by LTE and prior generations. It was estimated that the CC bandwidth can be up to 1 GHz or even more with mmWave [43]. In line with Shannon theory for achievable transmission rate, with better channel condition, wider CC bandwidth will yield faster rate. The 5G's claiming rate can be easily met with mmWave in this regard, albeit the specific frequency allocation and usage method of mmWave in 5G is still on discussion with international telecommunications union-radio communication (ITU-R).

Assuming the NOMA power allocation for each user as $P_i, i \in [1, K]$, the received signal is given by

$$\mathbf{y} = \mathbf{H}^H \mathbf{x} + \mathbf{n} = \sum_{i=1}^{K} P_i \mathbf{H}^H \mathbf{s} + \mathbf{n} \tag{1}$$

where $\mathbf{H} \in \mathbb{C}^{N \times K}$ is the channel model from N transmit antennas to K user terminals, $\mathbf{x} \in \mathbb{C}^{N \times 1}$ is the transmit information at the transmit side, which consists of the transmit signal $\mathbf{s}_i$ as well as the transmit power P_i. In addition, $\mathbf{n} \in \mathbb{C}^{K \times 1}$ yields the additive white Gaussian noise (AWGN). Moreover, without loss of generality, it is assumed that $N \geq K$. This is due to the fact that the transmit antenna number is usually larger than the receive antenna number in massive MIMO systems. It is also assumed that the transmit signal $\mathbf{s}$ is normalized, which means that each column of $\mathbf{s}$ obeys $\mathbb{E}[\mathbf{s}_i] = 0$, and $\mathbb{E}[\mathbf{s}_i \mathbf{s}_i^H] = 1$.

With this model in hand, to determinate the capacity performance of NOMA-mmWave-massive-MIMO systems, the channel model should be set forth. Given a constant normalized noise value within the channel assumption, capacity performance is largely determined by the allocated power to each user and the channel model [2].

B. The Proposed MmWave Channel Model

In line with prior studies from [12], [44], the mmWave channel model with a three dimensional (3D) transmission background has to take into consideration the channel gain, the AoD at the transmitter, and the AoA at the receiver. Taking an example, the mmWave channel response for the k-th user can be given as

$$\mathbf{h}_k = \sqrt{N} \left\{ \frac{\beta_k^0 \mathbf{d}(\theta_k^0) \mathbf{a}(\phi_k^0)}{\sqrt{1 + d_k^{\beta_k^0}}} + \sum_{i=1}^{M} \frac{\beta_k^i \mathbf{d}(\theta_k^i) \mathbf{a}(\phi_k^i)}{\sqrt{1 + d_k^{\beta_k^i}}} \right\}, \tag{2}$$

where $\mathbf{H} = [\mathbf{h}_1, \ldots, \mathbf{h}_K]$. Besides, integer $k \in [1, K]$ is the user index, and integer $i \in [1, M]$, the NLOS path index. β_k^i denotes the channel gain of user k for the i-th NLOS

[1]Note that NOMA decoding order can either with regard to the user orders [41], or with a reversed order with regard to the SNR [42]. Here in this study, we focus on the first scheme.

path, which can be assumed to obey a complex Gaussian distribution. Similarly, β_k^0 is the channel gain of the LOS path. M is the total number of NLOS paths. d_k denotes the distance between the BS and the k-th user. θ represents the normalized AoD of each path (by LOS or NLOS), which follows

$$\mathbf{d}(\theta) = \frac{1}{\sqrt{N}}[1, e^{-j\pi\theta}, \cdots, e^{-j\pi(N-1)\theta}]. \tag{3}$$

Similarly, the normalized AoA of each path follows

$$\mathbf{a}(\phi) = \frac{1}{\sqrt{N}}[1, e^{-j\pi\phi}, \cdots, e^{-j\pi(K-1)\phi}]^T. \tag{4}$$

However, according to prior findings in [46] and [47], mmWave transmission is highly susceptible to obstructions due to its vulnerable characteristic to diffraction and path loss. Thus mmWave beam highly relays on the LOS paths while applying in the wireless communications. With those antecedent studies in hand, by ignoring the NLOS components in (2) and assuming L LOS paths, a simplified model according to the UR-SP channel model [23], mmWave channel response for k-th user can be re-elaborated by

$$\mathbf{h}_k = \sqrt{N}\sum_{i=1}^{L}\frac{\beta_k^i \mathbf{d}(\theta_k^i)}{\sqrt{1+d_k^{\beta_k^i}}}. \tag{5}$$

Although the array steering vector (AoD vector) is included in the UR-SP channel model, the AoA factor is neglected in this model. Thus, in this study, we further extend the UR-SP model by taking the AoA vector into consideration. This results the channel response for the k-th user as

$$\mathbf{h}_k = \sqrt{N}\sum_{i=1}^{L}\frac{\mathbf{d}(\theta_k^i)\beta_k^i \mathbf{a}(\phi_k^i)}{\sqrt{1+d_k^{\beta_k^i}}}. \tag{6}$$

Additionally, by ignoring the difference bringing in by the shape of transmitter and receiver with an correlation free case both at transmit and receiver sides, the channel model $\mathbf{H}$ in high-dimensional matrix form can be given as

$$\mathbf{H} = \mathbf{DBA}, \tag{7}$$

where $\mathbf{D} \in \mathbb{C}^{N\times L}, \mathbf{B} \in \mathbb{C}^{L\times L}, \mathbf{A} \in \mathbb{C}^{L\times K}$. $\mathbf{B} = \eta\boldsymbol{\beta}$ with $\boldsymbol{\beta} = [\boldsymbol{\beta}_1, \boldsymbol{\beta}_2, \ldots, \boldsymbol{\beta}_L]$, and $\eta = [\eta_1, \ldots, \eta_k, \ldots, \eta_K]$. $\mathbf{D} = [\mathbf{d}(\theta_0), \ldots, \mathbf{d}(\theta_{L-1})], \mathbf{A} = [\mathbf{a}(\phi_0), \ldots, \mathbf{a}(\phi_{L-1})]^T$. Here η_k is the coefficient given as

$$\eta_k = \frac{\sqrt{N}}{\sqrt{1+d_k^{\beta_k^i}}}. \tag{8}$$

Here it is further assumed that the distance differences amongst different users can be absorbed into the β_k^i effects. This is because that with randomly generated $d_k^{\beta_k^i}$, η_k as an coefficient can be denoted with the randomly generated β_k^i in the analysis.

III. Capacity Analysis in the Noise-Dominated Low-SNR Regime

It is still intractable to directly analyze the capacity of the integrated NOMA-mmWave-massive-MIMO systems even with the simplified channel model due to the prohibited analysis complexity. That is, on the one hand, SIC is employed in NOMA to remove the interference and detect the desired signal. On the other hand, the mmWave channel model with multiple paths makes the analysis even tough. Thus, we divide the capacity analysis into low-SNR and high-SNR regimes, which can be adapted for various application scenarios such as cell edge, cell center, and etc. In addition, by summing up the two regimes, the majority conditions of cellular area can be covered.

In the low-SNR regime, the impact of the co-channel interference is trivial, and the dominant factor to each user's SINR value is the noise. In comparison, the dominant factor of SINR in the high-SNR regime is the co-channel interferences from other users. In this section, the capacity in the low-SNR regime is analyzed first by the deterministic equivalent method with the Stieltjes-Shannon transform [31], [47].

In the noise-dominated low-SNR regime, it is assumed that $\mathbf{D}$, $\mathbf{A}$ are the diagonal matrices with optimal beamforming of the NOMA-mmWave-massive-MIMO systems. This is a reasonable assumption due to the fact that only the direct beam targeting on the desired user can be the effective beam for transmission. All of the other AoD beams have no actual contribution for user k's transmission. In the low-SNR regime, the interference can be neglected compared to the noise power. The Stieltjes transform $S_{\mathbf{B}_N}(z)$ of matrix $\mathbf{B}_N$ can be employed for the capacity analysis in low-SNR regime,[2] which is defined as

$$\begin{aligned} S_{\mathbf{B}_N}(z) &= \frac{1}{N}tr(\mathbf{B}_N - z\mathbf{I}_N)^{-1} \\ &= \int \frac{1}{\lambda - z} dF_{\mathbf{B}_N}(\lambda) \\ &\xrightarrow{a.s.} \int \frac{1}{\lambda - z} dF_N(\lambda). \end{aligned} \tag{9}$$

In which the Hermitian non-negative definite matrix $\mathbf{B}_N$ is defined as

$$\mathbf{B}_N = \mathbf{H}\mathbf{H}^H = \mathbf{D}\mathbf{B}\mathbf{A}^2\mathbf{B}^H\mathbf{D}^H. \tag{10}$$

$z \in \mathbb{C} - \mathbb{R}^+ \equiv \{z \in \mathbb{C}, \Im(z) > 0\}$, and $\mathbf{I}_N$ is an identity matrix. In addition, $F_{\mathbf{B}_N}(\lambda)$ is the eigenvalue empirical distribution function (EDF) of $\mathbf{B}_N$. With N and K growing large, $F_{\mathbf{B}_N}(\lambda)$ converges to $F_N(\lambda)$ (the determinant eigenvalue CDF of $\mathbf{B}_N$) with probability 1 according to the Glivenko-Cantelli theorem [48].

The importance of the Stieltjes transform lies in its link to the Shannon transform $\mathcal{V}_{\mathbf{B}_N}(z)$ of $\mathbf{B}_N$, where the Shannon transform is directly linked with the capacity expression, which can be derived from the mutual information analysis in MIMO systems [37], [49].

[2]Note that here in this study, it is assumed that each user equipped with one receive antenna.

Theorem 1: The relationship between Stieltjes transform and Shannon transform of $\mathbf{B}_N$ can be given as

$$\begin{aligned}\mathcal{V}_{\mathbf{B}_N}(z) &= \int_0^{+\infty} \log\left(1+\frac{\lambda}{z}\right) dF_N(\lambda)\\ &= \int_z^{+\infty}\left(\frac{1}{w} - S_{\mathbf{B}_N}(-w)\right) dw. \end{aligned} \tag{11}$$

Proof: Please see Appendix A. ■

By assuming perfect channel state information at the receiver side (CSIR), the mutual information can be described by

$$I_{\mathbf{G}_N}(\sigma^2) = \mathbb{E}\left\{\log\det\left(\mathbf{I}_N + \frac{1}{\sigma^2}\mathbf{B}_N\right)\right\}. \tag{12}$$

In addition, the relationship between the Shannon transform and the ergodic mutual information is

$$I_{\mathbf{G}_N}(\sigma^2) = N\mathcal{V}_{\mathbf{B}_N}(\sigma^2). \tag{13}$$

Based on Theorem 1, the ergodic mutual information can be further determined by the Stieltjes transform on condition that $F_{\mathbf{B}}(\lambda) \rightarrow F_N(\lambda)$, which will be discussed in the following analysis. Before delving into detail analysis, a lemma and a hypothesis are given to clarify the constraints of this approach that used in this study.

Lemma 1: The sequences of $F_{\mathbf{D}}$, $F_{\mathbf{B}}$ and $F_{\mathbf{A}}$ (EDF of matrix $\mathbf{D}, \mathbf{B}, \mathbf{A}$) are tight, where $\mathbf{D}$ and $\mathbf{A}$ are the diagonal matrices as claimed before. Additionally, $\mathbf{B}$ is the random matrix with i.i.d. Gaussian entries of zero mean and covariance $\frac{1}{L}$.

Proof: Please see Appendix B. ■

The following hypothesis holds as well:

1) By defining $c = \frac{N}{K}$ and assuming $0 < a < b < \infty$, we have the following inequalities

$$a < \min_K \liminf_N c < \max_K \liminf_N c < b. \tag{14}$$

This hypothesis is to claim that the value of c has infimum and supremum with regards to K, N. This is reasonable by assuming that c is constant within the region $[0, +\infty]$. On this point, interested readers can refer to [31] and [32] and the references therein.

With all of those in hand, the mutual information can be straightforwardly obtained based on the Stieltjes transform of the channel matrix $\mathbf{B}_N$, which can be solved by using the link between $F_{\mathbf{B}_N}(\lambda)$ and $F_N(\lambda)$ of $\mathbf{B}_N$. Thus, the main problem is to find such a $F_N(\lambda)$. It is proved by prior studies [31], [47] that the difference between $F_{\mathbf{B}_N}(\lambda)$ and $F_N(\lambda)$ converges vaguely to zero:

$$S_{\mathbf{B}_N}(z) - S_N(z) \stackrel{a.s.}{\rightarrow} 0, \quad \text{for } z \in \mathbb{C} - \mathbb{R}^+, \tag{15}$$

where

$$S_N(z) \equiv \int_{\mathbb{R}^+} \frac{1}{\lambda - z} dF_N(\lambda) \tag{16}$$

By following the study in [50], given the noise variance σ^2 and the power matrix of each user $\mathbf{P}_k$, the deterministic equivalent of mutual information can be derived by using Lemma 1 and the hypothesis defined in (14) as

$$I(\sigma^2) = \bigcup_{\substack{\frac{1}{N}tr\mathbf{P}_k \leq P_k,\\ \mathbf{P}_k \geq 0,\\ k\in\mathcal{S}}} \left\{\sum_{k\in\mathcal{S}} C_k \leq \mathbb{E}\left\{\mathcal{V}_N(\mathbf{P}_k;\sigma^2)\right\}\right\}, \tag{17}$$

here $\mathcal{S} = \{1, \ldots, K\}$, C_k is the capacity of the k-th user. The Shannon transform is given by

$$\mathcal{V}_N(\mathbf{P}_k;\sigma^2) \stackrel{\text{def.}}{=} \frac{1}{N}\log\det\left(\mathbf{I}_N + \frac{1}{\sigma^2}\sum_{k\in\mathcal{S}} \mathbf{H}_k\mathbf{P}_k\mathbf{H}_k^H\right). \tag{18}$$

In this case, by assuming α a constant value, i.e., $0 < \alpha < \infty$, the spectral norm satisfies

$$\max\{\|\mathbf{D}\|, \|\mathbf{A}\|, \|\mathbf{H}\mathbf{H}^H\|\} \leq \alpha. \tag{19}$$

By following the prior studies in [31], [34], the deterministic expression of the ergodic capacity can be given as

$$\begin{aligned} C &\leq \sum_{k=1}^K \mathbb{E}\left\{\mathcal{V}_N(\mathbf{P}_k;\sigma^2)\right\}\\ &\stackrel{\text{a. s.}}{\rightarrow} \frac{1}{N}\sum_{k=1}^K \log\det(\mathbf{I} + ce_k(-\sigma^2)\mathbf{A}_k^2\mathbf{P}_k)\\ &\quad + \frac{1}{N}\log\det(\mathbf{I} + \sum_{k=1}^K f_k(-\sigma^2)\mathbf{D}_k^2)\\ &\quad - \sigma^2\sum_{k=1}^K f_k(-\sigma^2)e_k(-\sigma^2). \end{aligned} \tag{20}$$

where $e_k(-\sigma^2)$ and $f_k(-\sigma^2)$ are the unique positive solutions of the following symmetric equalities

$$e_k(-\sigma^2) = \frac{1}{N}tr\mathbf{D}_k^2(\sigma^2[\mathbf{I} + \sum_{k=1}^K f_k(-\sigma^2)\mathbf{D}_k^2])^{-1}, \tag{21}$$

$$f_k(-\sigma^2) = tr\mathbf{A}_k\mathbf{P}_k\mathbf{A}_k(\sigma^2[\mathbf{I} + ce_k(-\sigma^2)\mathbf{A}_k\mathbf{P}_k\mathbf{A}_k])^{-1}. \tag{22}$$

The sum rate supremum of the NOMA-mmWave-massive-MIMO systems can be addressed by (20) with $e_k(-\sigma^2)$ and $f_k(-\sigma^2)$ the unique solutions of the equalities given in (21) and (22), where the iterative algorithm to obtain these solutions can be found by [32], [34], and [52].

As discussed before, this deterministic equivalent method is only valid in the low-SNR scenario. In the following analysis, we further focus the study in high SNR regime. In that case, the interferences mostly come from neighboring users within the user group. Then after SIC, prior deterministic equivalent method with Shannon-Stieltjes transform is not valid for analysis. This is because that with Shannon-Stieltjes transform, it is assumed that for each user, only the channel noise is existing. Thus given the transmission and channel noise power values, only the channel matrix is the determinant variable for achievable capacity. The high-SNR capacity analysis is addressed in the following section. Finally by summarizing these two regimes, we can approach the majority scenarios in integrating NOMA-mmWave-massive-MIMO systems. The comprehensive closed-form capacity expression in the existence of co-channel interference and channel noise is way complex, which is left for further study.

IV. Capacity Analysis in the Interference-Dominated High-SNR Regime

The high-SNR regime is investigated in this section. To surround the systems' capacity in high-SNR regime, an alternative method with statistics and probability analysis is adopted based on the channel distribution analysis. Firstly, by employing the SIC [41] to perfectly cancel the co-channel interferences with higher orders, the SINR of user k can be given as

$$\begin{aligned} SINR_k &\Leftrightarrow \frac{P_k \mathbf{H}\mathbf{H}^H}{\sum_{k'=1,k'\neq k}^{K} P_{k'}\mathbf{H}\mathbf{H}^H + \sigma^2} \\ &\overset{SIC}{\Leftrightarrow} \frac{P_k \mathbf{H}\mathbf{H}^H}{\sum_{k'=1}^{k-1} P_{k'}\mathbf{H}\mathbf{H}^H + \sigma^2}. \end{aligned} \tag{23}$$

Here the first expression is logically defined as the received SINR for each user k without the SIC. After the SIC, the second equality can be straightforwardly arrived. The capacity of the NOMA-mmWave-massive-MIMO systems within high-SNR regime then, can be approximated as

$$\begin{aligned} C &= \sum_{k=1}^{K} \mathbb{E}\left\{\log\det\left(\mathbf{I}_N + \frac{P_k \mathbf{H}\mathbf{H}^H}{\sum_{k'=1}^{k-1} P_{k'}\mathbf{H}\mathbf{H}^H + \sigma^2}\right)\right\} \\ &\overset{high\ SNR}{\approx} \sum_{k=1}^{K} \mathbb{E}\left\{\log\det\left(\mathbf{I}_N + \frac{P_k \mathbf{H}\mathbf{H}^H}{\sum_{k'=1}^{k-1} P_{k'}\mathbf{H}\mathbf{H}^H}\right)\right\}. \end{aligned} \tag{24}$$

In the following, a tractable capacity expression is derived by employing the tools of statistics and probability analysis method [35]. First of all, the capacity expression can be divided into the power allocation part and channel characteristic part by Theorem 4.1.

Theorem 2: The ergodic capacity of NOMA-mmWave-massive-MIMO systems in high-SNR regime is

$$\begin{aligned} C = \frac{1}{\ln 2}\sum_{k=1}^{K}\Bigg\{ &\ln\left(\frac{\sum_{k'=1}^{k} P_{k'}}{\sum_{k'=1}^{k} P_{k'} - P_k}\right) \\ &+ \ln\int_0^{+\infty}\lambda f(\lambda)d\lambda\Bigg\}, \end{aligned} \tag{25}$$

where λ is the eigenvalue of $\mathbf{H}\mathbf{H}^H$, and $f(\lambda)$ is the PDF of λ.

Proof: Please see Appendix C. ■

As shown, the first part of Theorem 2 is about the power ratio with NOMA scheme, where the second part is about the eigenvalue and its PDF of $\mathbf{H}\mathbf{H}^H$. Once the NOMA power allocation is given, the first part will be determined, and the capacity mainly depends on the second part with $f(\lambda)$. The exact expression of $f(\lambda)$ is pursued and given by the following lemma 2.

Lemma 2: By exploring the knowledge of probability analysis, the unconditional PDF of $\mathbf{H}\mathbf{H}^H$ can be calculated as

$$\begin{aligned} f(\lambda) &= \frac{1}{\prod_{i=1}^{L}\Gamma^2(L-i+1)\prod_{i=1}^{L}\Gamma(N-i+1)L} \\ &\quad\times \sum_{j=L-K+1}^{L}\sum_{i=1}^{L}(-1)^{i+j}\frac{\lambda^{K-L+j-1}}{\Gamma(K-L+j)}\det(\mathbf{M})N_\lambda(i). \end{aligned} \tag{26}$$

where $\mathbf{M}_{i,j}$ is the (i,j)-th minor of matrix $\mathbf{M} \in \mathbb{C}^{L\times L}$, whose entry is given as

$$\mathbf{M}_{i,j} = \Gamma(i+j-1)\Gamma(N-L+j). \tag{27}$$

Additionally, the expression of $N_\lambda(j)$ is

$$N_\lambda(i) = \int_0^{+\infty} 4x^{N+L-2K+i-2}e^{-\frac{\lambda}{x^2}}K_{L-N+i-1}(2x)dx, \tag{28}$$

with $K_m(n)$ is the modified Bessel function of its second kind.

Proof: Please see Appendix D. ■

The exact capacity expression is acquired by substituting lemma 2 into (25), and $\int_0^{+\infty}\lambda f(\lambda)d\lambda$ is given as (29), shown at the bottom of the next page.

As shown in (25) and (29), although the exact expression of the capacity is derived, but the expression is complex as a non closed-form expression with integral. Fortunately, to obtain the closed-form expression of the eigenvalues' PDF of $\mathbf{H}\mathbf{H}^H$, the study from [52] gives an asymptotic expression under a similar condition. By following the deduction procedure, although it is still difficult to obtain the closed-form expression under condition $N \neq K \neq L$, but when $N = L = K$, the expression is reduced to [35]

$$f(\lambda) = \frac{1}{\pi}\sqrt{g^2(\lambda) + \frac{1}{4\lambda^2 g(\lambda)}}, \tag{30}$$

where $g^2(\lambda)$ is given as [35]

$$\begin{aligned} g^2(\lambda) &= \frac{\sqrt[3]{64^2\lambda^8}(1-i'\sqrt{3})}{384\lambda^4}\sqrt[3]{\frac{-27+\sqrt{27^2-27\frac{16^2}{\lambda}}}{2}} \\ &\quad+ \frac{\sqrt[3]{64^2\lambda^8}(1+i'\sqrt{3})}{384\lambda^4}\sqrt[3]{\frac{-27-\sqrt{27^2-27\frac{16^2}{\lambda}}}{2}}. \end{aligned} \tag{31}$$

Here i' yields the unit imaginary number. On condition that $f(\lambda) \geq 0$, by combining the (30) and (31), we have $\lambda_{max} = \frac{16^2}{27}$. This gives the expression of $f(\lambda)$ as

$$\begin{aligned} f(\lambda) &= \frac{\left(1+i'\sqrt{3}\right)\sqrt[3]{\lambda^8}\sqrt[3]{-\sqrt{729-\frac{6912}{\lambda}}-27}}{24\sqrt[3]{2}\lambda^4} \\ &\quad+ \frac{\left(1-i'\sqrt{3}\right)\sqrt[3]{\lambda^8}\sqrt[3]{\sqrt{729-\frac{6912}{\lambda}}-27}}{24\sqrt[3]{2}\lambda^4}. \end{aligned} \tag{32}$$

Thus by substituting (32) into (25), the ergodic capacity can be rewritten as

$$C = \frac{1}{\ln 2}\sum_{k=1}^{K}\left\{ \ln\left(\frac{\sum_{k'=1}^{k} P_{k'}}{\sum_{k'=1}^{k} P_{k'} - P_k}\right) + \ln \int_0^{\frac{16^2}{27}} \lambda f(\lambda) d\lambda \right\}, \tag{33}$$

where $f(\lambda)$ is given by (32).

In summary, the exact capacity expression defined in (25) is well suited for general cases in NOMA-mmWave-massive-MIMO systems despite its high computation complexity. For the special case that $N = L = K$, the asymptotic capacity expression with (32) can be employed, which will be verified through numerical results.

V. Numerical Results

The capacity performance of NOMA-mmWave-massive-MIMO systems is evaluated in this section. The low-SNR regime analysis is evaluated firstly. The matrix $\mathbf{B}$ is randomly generated with zero mean and covariance $\frac{1}{L}$, in line with the hypothesis and assumptions of the prior analysis. With SNR value given by 0 dB and -10 dB (the SNR value is given by averaged over all users in each simulation), the capacity performance is given by Fig. 2. As shown here, with SNR increasing, the achievable capacity is also increased. In addition, with NOMA user number increasing, the capacity difference between 0 dB and -10 dB becomes even greater. This is due to the fact that, in this simulation, it is assumed that the user allocated power value increases with user index increasing. Thus more user yields greater averaged power value (total allocated power divided by engaged user number), which in turns, better capacity performance. It is worth noting that the capacity performance of the NOMA-mmWave-massive-MIMO systems outperforms the existing LTE systems ($0.07 \sim 0.12$ bits/s/Hz of the cell-edge, which yields the low-SNR regime) [53]. For instance, by 10 users and -10 dB, the achievable capacity value is almost 10 times compared with prior LTE systems in low-SNR regime. This is mainly due to the NOMA encoding scheme with multiple users of each frequency resource block, and the power allocation method of this simulation.

To verify the correctness of the PDF deductions in this study, the exact eigenvalue PDF expression in (26) is compared with the asymptotic PDF expression in (32). The results are shown in Fig. 3 and Fig. 4 for $N = L = K = 2$ and $N = L = K = 6$, respectively. By observing Fig. 3 and Fig. 4, it is clear that the asymptotic PDF expression is in good

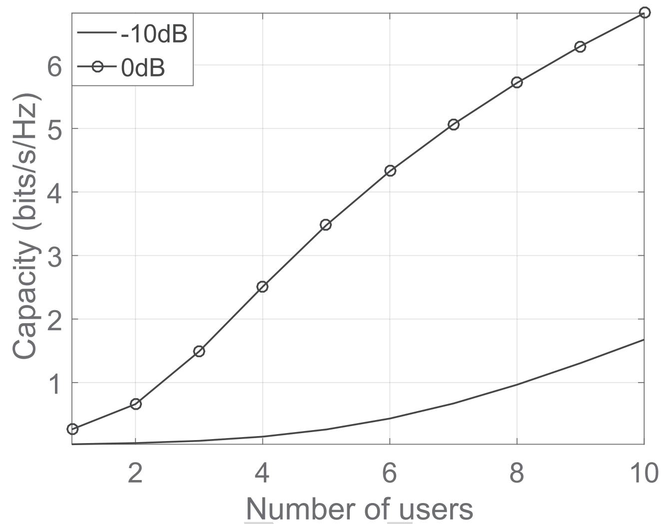

Fig. 2. Capacity performance of the low-SNR scenario. The calculation is based on (20), (21) and (22).

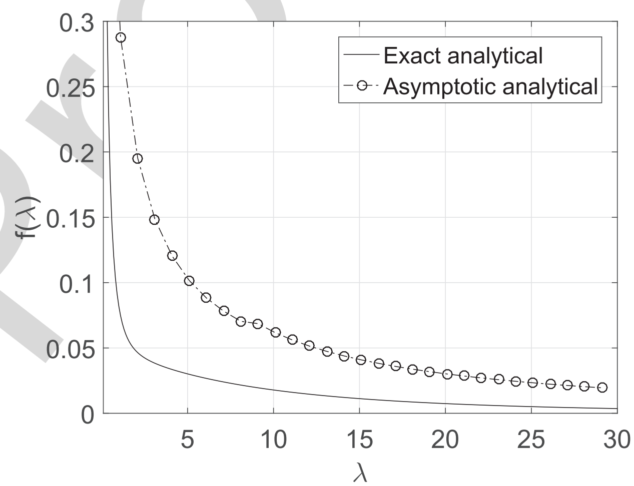

Fig. 3. Analytical comparison of the exact and asymptotic eigenvalue PDFs ($N = L = K = 2$). The exact analytical curve is based on (26), where asymptotic analytical curve is based on (32).

$$\begin{aligned}\int_0^{+\infty} \lambda f(\lambda) d\lambda &= \int_0^{+\infty} \frac{\lambda}{\prod_{i=1}^{L}\Gamma^2(L-i+1)\prod_{i=1}^{L}\Gamma(N-i+1)L} \\ &\quad \times \sum_{j=L-K+1}^{L}\sum_{i=1}^{L}(-1)^{i+j}\frac{\lambda^{K-L+j-1}}{\Gamma(K-L+j)}\det(\mathbf{M})N_\lambda(i)d\lambda \\ &= \frac{1}{\prod_{i=1}^{L}\Gamma^2(L-i+1)\prod_{i=1}^{L}\Gamma(N-i+1)L}\sum_{j=L-K+1}^{L}\sum_{i=1}^{L}(-1)^{i+j} \\ &\quad \times \int_0^{+\infty}\frac{\det(\mathbf{M})\lambda^{K-L+j}}{\Gamma(K-L+j)}N_\lambda(i)d\lambda. \end{aligned} \tag{29}$$

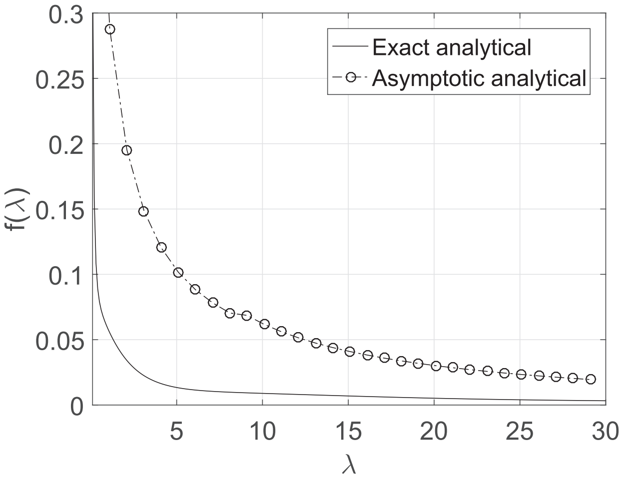

Fig. 4. Comparison of the exact and asymptotic eigenvalue PDFs ($N = L = K = 6$). The exact analytical curve is based on (26), where asymptotic analytical curve is based on (32).

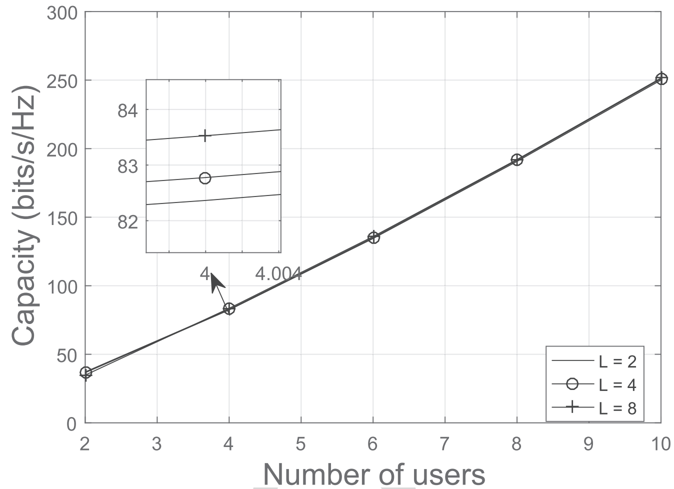

Fig. 6. Capacity performance of high-SNR scenario with the exact eigenvalue PDF ($N = 20$). The calculation is based on (25) and (29).

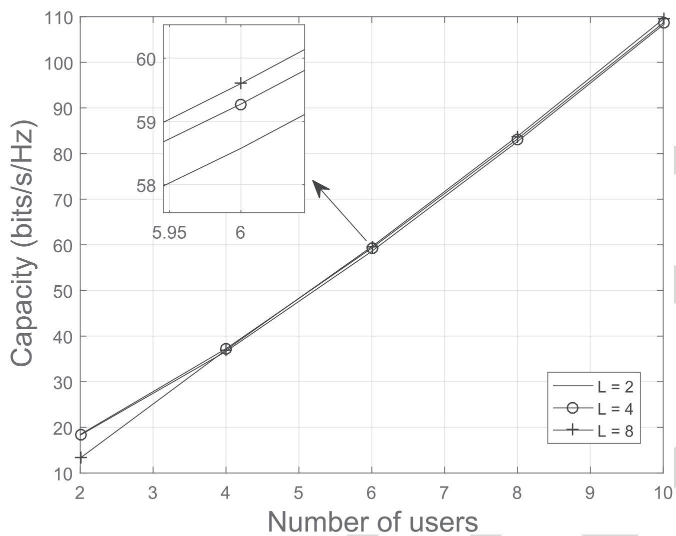

Fig. 5. Capacity performance of high-SNR scenario with the exact eigenvalue PDF ($N = 10$). The calculation is based on (25) and (32).

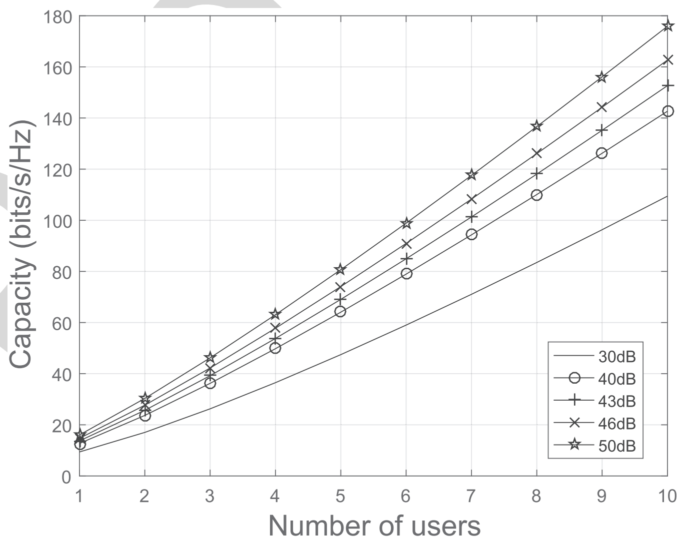

Fig. 7. Capacity performance of high-SNR scenario with the asymptotic eigenvalue PDF. The calculation is based on (33) and (29).

agreement with the exact eigenvalue PDF expression in low and high eigenvalue regions. However, there is a disagreement within other region. In addition, the disagreement grows large with the numbers (N, L, K) growing. Thus the asymptotic PDF is more feasible to adopt with small N, L, K values. The asymptotic expression, albeit results in larger difference with numbers (N, L, K) growing large, but consumes much lesser time while adopting. For instance, to plot the Fig. 4 with $N = L = K = 6$ (Intel Xeon Processor E3-1241 v3, 8 M Cache, 3.50 GHz, 16 G RAM), the consuming time is 4.913563 s with exact PDF expression. In contrast, the asymptotic PDF expression consumes 0.000655 s.

The capacity performances of NOMA-mmWave-massive-MIMO systems with the exact PDF expression are shown in Fig. 5 and Fig. 6 for $N = 10$ and $N = 20$, respectively. The SNR is set to be 30 dB for both simulations. By comparing these two figures, it is clear that with antenna number growing, the capacity performance is enhanced. The reason behind is that more transmit antennas bring in more degree of freedom [4], which is in tune with previous studies [2], [32]. In addition, it is observed that little capacity improvement can be achieved by increasing the number of LOS paths. This is mainly because of the channel hardening effects [54]. Besides, the co-channel interferences from neighboring users and the correlative effects at transmit and receiver sides are enhanced with LOS path number increasing.

Fig. 7 further verifies the relationship between the high-SNR capacity and SNR according to the asymptotic expression. Simulation results show that the high-SNR capacity of the NOMA-mmWave-massive-MIMO systems significantly outperforms the existing LTE systems (with a capacity of 30 bit/s/Hz) [53]. For example, a 240% capacity improvement when $K = 10$, SNR $= 50$ dB. Thus, it is clear that the integration of the three key technologies demonstrates dramatic potential to meet the SE requirement of 5G. On the other hand, it is shown that although the capacity increases monotonically as the transmit power increasing; the performance improvement becomes saturated when the SNR is sufficiently high. The reason is that co-channel interferences from neighboring users are also increased as the transmit power increasing. Although the capacity improvement can be obtained by just increasing the power, simulation results demonstrate that there is a tradeoff between energy consumption and capacity improvement.

VI. Discussion and Conclusion

The capacity performance of NOMA-mmWave-massive-MIMO systems was investigated in this study. We divided the capacity analysis into the noise-dominated low-SNR regime and the interference-dominated high-SNR regime. The deterministic expressions were given by the analysis for both low-SNR and high-SNR regimes. Additionally, a low-complexity asymptotic capacity expression was given based on the asymptotic PDF of channel eigenvalues. Simulation results indicated that enormous capacity improvement can be achieved compared to the existing LTE systems. We also found that the user number has a strong positive impact on the capacity improvement. This is due to the non-orthogonal user multiplexing in the same frequency resource block enabled by NOMA. In comparison, little capacity improvement can be achieved by increasing the number of LOS paths. Numerical results also revealed that there exists a tradeoff between energy consumption and capacity improvement.

In addition, with much wider bandwidth that provided by mmWave, even higher systems' sum rate increment can be obtained, which yields an attractive perspective for 5G. For instance, as the possible 1 GHz CC bandwidth, under ideal condition, the achievable throughput will be $100 \sim 200$ Gbit/s with the NOMA-mmWave-massive MIMO systems. This integration results in negative effect to the systems' deployment by its denser BS deployment with massive MIMO and vulnerable transmission beams with mmWave. Albeit the deployment of small cell BS with massive MIMO is on the test, but the various obstructions will bring in great challenges for integrating those small cells with mmWave. The SIC encoding equipment of NOMA is another challenge for application at the receiver side. Other than the theoretical analysis in this paper, the optimal power allocation scheme of NOMA-mmWave-massive-MIMO systems can be another interesting topic, which is left for future study.

Appendix A

Proof: To prove the relationship between Shannon transform and Stieltjes transform, some notes should be stated beforehand.

Note 1: use ln for the log base e. For $b > 0$, we have

$$\ln(1+b) = \int_0^1 \frac{b}{1+bt} dt. \tag{34}$$

Note 2: Instead of the distribution function $dF(x)$, for convenience, we use $\rho(x)dx$ as the density. In this case, for $z \to \infty$, say in the upper-half plane, we have

$$\int_0^{+\infty} \rho(\lambda) d\lambda = 1. \tag{35}$$

Firstly, the Shannon transform is defined as

$$\mathcal{V}(x) = \int_0^{+\infty} \log(1+\frac{\lambda}{x})\rho(\lambda) d\lambda. \tag{36}$$

In this case, the differential result of this equality can be given as

$$\frac{d\mathcal{V}(x)}{dx} = -\frac{1}{\log e}\int_0^{+\infty} \frac{\frac{\lambda}{x^2}\rho(\lambda)}{1+\frac{\lambda}{x}} d\lambda. \tag{37}$$

Furthermore, by multiplying x on both sides, we have

$$\begin{aligned} x\frac{d\mathcal{V}(x)}{dx} &= -\frac{1}{\log e}\int_0^{+\infty} \frac{\lambda\rho(\lambda)}{x+\lambda} d\lambda \\ &= -\frac{1}{\log e}\int_0^{+\infty} \frac{(\lambda+x-x)\rho(\lambda)}{x+\lambda} d\lambda \\ &= -\frac{1}{\log e}\left(1 - x\int_0^{+\infty} \frac{\rho(\lambda)}{x+\lambda} d\lambda\right). \end{aligned} \tag{38}$$

It is noticed that a Stieltjes transform appeared by the last part of the equality's right side. This result gives

$$x\frac{d\mathcal{V}(x)}{dx} = -\frac{1}{\log e}\left(1 - xS(-x)\right). \tag{39}$$

Which is the link between Shannon transforma and Stieltjes transform given by [55] and similar literatures. In addition, it is noticed that in alternative literature (for instance, [31], [47]), the $\log e$ factor is omitted to arrive the equivalence given by Theorem 3.1. Thus by omitting the factor and unpacking the log according to (34), we have,

$$\begin{aligned} \mathcal{V}(x) &\approx \int_0^{+\infty} \rho(\lambda)\int_0^1 \left(\frac{\frac{\lambda}{x}}{1+\frac{\lambda}{x}t} dt\right) d\lambda \\ &= \int_0^{+\infty} \rho(\lambda)\left(\int_0^1 \frac{\lambda}{x+\lambda t} dt\right) d\lambda. \end{aligned} \tag{40}$$

Let $t = \frac{1}{\omega}$, since $t \in [0,1], \omega \in [0,\infty)$, we see that

$$\begin{aligned} \mathcal{V}(x) &= \int_0^{+\infty} \rho(\lambda)\left(\int_0^1 \frac{\lambda}{x+\lambda\frac{1}{\omega}} d\frac{1}{\omega}\right) d\lambda \\ &= \int_0^{+\infty} \rho(\lambda)\left(\int_1^{\infty}\left(\frac{\lambda}{\omega x+\lambda}\right)\frac{d\omega}{\omega}\right) d\lambda. \end{aligned} \tag{41}$$

By changing the variable with $\Omega = \omega x$, whereas $\omega = \frac{\Omega}{x}, d\omega = \frac{d\Omega}{x}$, and exchanging the λ and ω integration, we have

$$\begin{aligned} \mathcal{V}(x) &= \int_0^{+\infty} \rho(\lambda)\left(\int_1^{\infty}\left(\frac{\lambda}{\omega x+\lambda}\right)\frac{d\omega}{\omega}\right) d\lambda \\ &\overset{a}{=} \int_0^{+\infty} \rho(\lambda)\left(\int_x^{\infty}\left(\frac{\lambda}{\Omega+\lambda}\right)\frac{1}{\Omega}d\Omega\right) d\lambda \\ &= \int_0^{+\infty} \frac{1}{\Omega}\rho(\lambda)\left(\int_x^{\infty}\left(\frac{\lambda+\Omega-\Omega}{\Omega+\lambda}\right)d\Omega\right) d\lambda \\ &= \int_x^{+\infty}\left(\frac{1}{\Omega}\rho(\lambda)d\lambda - \int_o^{\infty}\left(\frac{\rho(\lambda)}{\Omega+\lambda}\right)d\lambda\right) d\Omega, \end{aligned} \tag{42}$$

where a denotes the exchange of $\mathbf{\Omega}$ with ωx. Thus consequently we have

$$\mathcal{V}(x) = \int_{x}^{+\infty} \left(\frac{1}{\omega} - S(-\omega)\right) d\omega. \tag{43}$$

This completes the proof. ∎

Appendix B

Proof: As the proof procedures are similar for $F_{\mathbf{D}}$, $F_{\mathbf{B}}$, and $F_{\mathbf{A}}$, here we only give the proof of the tightness of $F_{\mathbf{A}}$. Without loss of generality, assuming $\mathbf{A} \sim \mathcal{CN}(\boldsymbol{\mu}, \boldsymbol{\Sigma})$, its PDF can be given as

$$p(x; \boldsymbol{\mu}, \boldsymbol{\Sigma}) = \frac{1}{\sqrt{(2\pi)^2|\boldsymbol{\Sigma}|}} \exp\left(-\frac{1}{2}(\mathbf{x}-\boldsymbol{\mu})^T \boldsymbol{\Sigma}^{-1}(\mathbf{x}-\boldsymbol{\mu})\right). \tag{44}$$

The CDF can be given while doing the integral to $\mathbf{x}$, which is

$$F(x; \boldsymbol{\mu}, \boldsymbol{\Sigma}) = \frac{1}{\sqrt{(2\pi)^2|\boldsymbol{\Sigma}|}} \int_{-\infty}^{x_1} \cdots \int_{-\infty}^{x_k} \times \exp\left(-\frac{1}{2}(\mathbf{x}-\boldsymbol{\mu})^T \boldsymbol{\Sigma}^{-1}(\mathbf{x}-\boldsymbol{\mu})\right) dx_1 \ldots dx_k. \tag{45}$$

Hence by following the proof procedure of sequence tightness, we have proof that for $\epsilon > 0$ and $N_\epsilon > 0$, for all k, the following inequality holds

$$\begin{aligned} &F_k(N_\eta; \boldsymbol{\mu}, \boldsymbol{\Sigma}) \\ &= \frac{1}{\sqrt{(2\pi)^2|\boldsymbol{\Sigma}|}} \int_{-\infty}^{N_{\epsilon 1}} \cdots \int_{-\infty}^{N_{\epsilon k}} \\ &\quad \times \exp\left(-\frac{1}{2}(\mathbf{x}-\boldsymbol{\mu})^T \boldsymbol{\Sigma}^{-1}(\mathbf{x}-\boldsymbol{\mu})\right) dN_{\epsilon 1} \ldots dN_{\epsilon k} \\ &> 1 - \eta. \end{aligned} \tag{46}$$

That is

$$\begin{aligned} \epsilon &> 1 - F_k(N_\epsilon; \boldsymbol{\mu}, \boldsymbol{\Sigma}) \\ &= 1 - \frac{1}{\sqrt{(2\pi)^2|\boldsymbol{\Sigma}|}} \int_{-\infty}^{N_{\epsilon 1}} \cdots \int_{-\infty}^{N_{\epsilon k}} \\ &\quad \times \exp\left(-\frac{1}{2}(\mathbf{x}-\boldsymbol{\mu})^T \boldsymbol{\Sigma}^{-1}(\mathbf{x}-\boldsymbol{\mu})\right) dN_{\epsilon 1} \ldots dN_{\epsilon k}. \end{aligned} \tag{47}$$

As known, $-\frac{1}{2}(\mathbf{x}-\boldsymbol{\mu})^T \boldsymbol{\Sigma}^{-1}(\mathbf{x}-\boldsymbol{\mu})$ is a quadratic form of $\mathbf{x}$, and $\boldsymbol{\Sigma}$ is positive definite. Thus for any $x \neq \mu$, we have

$$-\frac{1}{2}(\mathbf{x}-\boldsymbol{\mu})^T \boldsymbol{\Sigma}^{-1}(\mathbf{x}-\boldsymbol{\mu}) < 0. \tag{48}$$

This implies that both $p(x; \boldsymbol{\mu}, \boldsymbol{\Sigma})$ and $F(x; \boldsymbol{\mu}, \boldsymbol{\Sigma})$ are monotone decreasing functions of x. Thus by assuming a vector $\mathbf{b}$ with $0 < b \leq N$, when $b \to 0$ we have

$$\epsilon > 1 - F_k(b; \boldsymbol{\mu}, \boldsymbol{\Sigma}) \to \epsilon > 1 - F_k(N_\epsilon; \boldsymbol{\mu}, \boldsymbol{\Sigma}). \tag{49}$$

By following the Glivenko-Cantelli theorem, we can arrive at the tightness conclusion with EDF $F_{\mathbf{A}}$. The proof of the tightness characteristics of sequences $F_{\mathbf{D}}$ and $F_{\mathbf{B}}$ is similar, which is omitted here.

This completes the proof. ∎

Appendix C

Proof: As stated by (24), the achievable transmission rate of each user k can be given as

$$C_k = \mathbb{E}\left\{\log\det\left(\mathbf{I}_N + \frac{P_k \mathbf{H}\mathbf{H}^H}{\sum_{k'=1}^{k-1} P_{k'}\mathbf{H}\mathbf{H}^H}\right)\right\}. \tag{50}$$

While reducing of fractions to a common denominator, we have

$$C_k = \mathbb{E}\left\{\log\det\left(\frac{\sum_{k'=1}^{k-1} P_{k'}\mathbf{H}\mathbf{H}^H + P_k\mathbf{H}\mathbf{H}^H}{\sum_{k'=1}^{k-1} P_{k'}\mathbf{H}\mathbf{H}^H}\right)\right\}. \tag{51}$$

Additionally, this can be further written as

$$\begin{aligned} C_k &= \mathbb{E}\left\{\log\det\left(\frac{\sum_{k'=1}^{k} P_{k'}\mathbf{H}\mathbf{H}^H}{\sum_{k'=1}^{k-1} P_{k'}\mathbf{H}\mathbf{H}^H}\right)\right\} \\ &= \mathbb{E}\left\{\log\det\left(\frac{\sum_{k'=1}^{k} P_{k'}\mathbf{H}\mathbf{H}^H}{\sum_{k'=1}^{k} P_{k'}\mathbf{H}\mathbf{H}^H - P_k\mathbf{H}\mathbf{H}^H}\right)\right\} \\ &= \log\left\{\left(\frac{\sum_{k'=1}^{k} P_{k'}}{\sum_{k'=1}^{k} P_{k'} - P_k}\right)\mathbb{E}\left(\det\mathbf{H}\mathbf{H}^H\right)\right\}. \end{aligned} \tag{52}$$

Exchanging the base of logarithm to the last equality, and following the prior studies by [27], [42], and [57] will yield the following equality

$$\begin{aligned} C_k &= \log\left\{\left(\frac{\sum_{k'=1}^{k} P_{k'}}{\sum_{k'=1}^{k} P_{k'} - P_k}\right)\mathbb{E}\left(\det\mathbf{H}\mathbf{H}^H\right)\right\} \\ &= \frac{1}{\ln 2}\left\{\ln\left(\frac{\sum_{k'=1}^{k} P_{k'}}{\sum_{k'=1}^{k} P_{k'} - P_k}\right)\right. \\ &\quad \left. + \ln\int_0^{+\infty} \lambda f(\lambda)\right\}. \end{aligned} \tag{53}$$

While summarizing the achievable rate to all K users, it will be the result in *Theorem 4.1*.

This completes the proof. ∎

Appendix D

Proof: Here the eigenvalue decomposition (ED) method is utilized. The difference between the singular eigenvalue decomposition (SVD) and ED methods is that, SVD yields the rotation transform while ED is not. Since $\mathbf{B}$ is a normal square random matrix, ED will yield two unitary matrices plus a diagonal matrix. The analysis is simplified via this method. Inspired by the prior studies in [27], [57], and [58], the eigenvalue decomposition of $\mathbf{B}$ can be given as

$$\mathbf{B} = \mathbf{Q}\mathbf{D}_1\mathbf{Q}^H, \tag{54}$$

whereas $\mathbf{Q}$ is the unitary matrix, and $\mathbf{D}_1$ is the diagonal matrix. With this in hand, for $\mathbf{BA}$, the following equality holds

$$\begin{aligned} (\mathbf{BA})(\mathbf{BA})^H &= \mathbf{Q}\mathbf{D}_1\mathbf{Q}^H\mathbf{A}\mathbf{A}^H\mathbf{Q}\mathbf{D}_1^H\mathbf{Q}^H \\ &= \mathbf{Q}\mathbf{D}_1\tilde{\mathbf{A}}\tilde{\mathbf{A}}^H\mathbf{D}_1^H\mathbf{Q}^H \triangleq \mathbf{Q}\mathbf{W}_0\mathbf{Q}^H. \end{aligned} \tag{55}$$

This gives the matrix $\mathbf{W}_0$ a central Wishart matrix with K non-zero eigenvalues defined as $0 < \chi_1 < \ldots < \chi_K < \infty$. By denoting the eigenvalues of $\mathbf{BB}^H$ as $0 < \upsilon_1 < \ldots < \upsilon_L < \infty$, in line with prior study [56], the CDF of the largest eigenvalue of $(\mathbf{BA})(\mathbf{BA})^H$ conditioned on $\mathbf{B}$ can be given as [56], [58]

$$F_{\chi_{max}}(x|\mathbf{B}) = \frac{(-1)^{K(L-K)}\det(\Delta(x))}{\det(\mathbf{V})\prod_{i=1}^{K}\Gamma(K-i+1)}. \tag{56}$$

where $\Delta(x)$ is an $L \times L$ matrix with entries

$$\Delta(x)_{i,j} = \begin{cases} (-\dfrac{1}{\upsilon_j})^{L-K-i}, & \text{for } i \le L-K, \\ \upsilon_j^{L-i+1}\gamma(L-i+1, \dfrac{xL}{\upsilon_j}), & \text{for } i > L-K. \end{cases} \tag{57}$$

Additionally, $\mathbf{V}$ is a $L \times L$ matrix defined as [27]

$$\det(\mathbf{V}) = \left(\prod_{i=1}^{L}\upsilon_i^K\right)\prod_{1\le l\le k\le L}\left(\frac{1}{\upsilon_k}-\frac{1}{\upsilon_l}\right). \tag{58}$$

By some manipulations with regard to the Vandermonde determinant identity, it can be further written as

$$\begin{aligned}\det(\mathbf{V}) &= \left(\prod_{i=1}^{L}\upsilon_i^K\right)(-1)^{\frac{L(L-1)}{2}}\frac{\prod_{1\le i\le j\le L}(\upsilon_j-\upsilon_i)}{\prod_{i=1}^{L}\upsilon_i^{L-1}} \\ &= \left(\prod_{i=1}^{L}\upsilon_i^{K-L+1}\right)\prod_{1\le i\le j\le L}(\upsilon_i-\upsilon_j) \end{aligned}\tag{59}$$

On the other hand, by following the prior studies in [57] and [59], for the square matrix $\mathbf{B} \in \mathbb{C}^{L\times L}$ here in this paper, the joint PDF of the eigenvalue $0 < \upsilon_1 < \ldots < \upsilon_L < \infty$ of the matrix constituted by $\mathbf{BB}^H$ is given by

$$f_\upsilon(\mathbf{D}_1) = \frac{e^{-\sum_{i=1}^{L}\upsilon_i}\prod_{i<j}^{L}(\upsilon_j-\upsilon_i)^2}{\prod_{i=1}^{L}\Gamma(L-i+1)^2}. \tag{60}$$

To this end, the unconditional CDF of $0 < \chi_1 < \ldots < \chi_K < \infty$ will be

$$F_{\chi_{max}}(x) = \int_{\mathcal{U}} F_{\chi_{max}}(x|\mathbf{B})f_\upsilon(\mathbf{D}_1)d\upsilon_1,\ldots d\upsilon_L, \tag{61}$$

where $\mathcal{U} \triangleq \{0 < \chi_1 < \ldots < \chi_K < \infty\}$, this gives

$$F_{\chi_{max}}(x) = \frac{(-1)^{K(L-K)}\det(\mathbf{D}(x))}{\prod_{k=1}^{K}\Gamma(K-k+1)\prod_{i=1}^{L}\Gamma(L-i+1)^2}, \tag{62}$$

where $\mathbf{D}(x)$ is given as

$$\begin{aligned}\mathbf{D}(x) = &\int_{\mathcal{U}}\det(\Delta(x))e^{-\sum_{i=1}^{L}\upsilon_i} \\ &\times\prod_{i=1}^{L}\upsilon_i^{L-K-1}\prod_{i<j}^{L}(\upsilon_i-\upsilon_j)d\upsilon_1,\ldots d\upsilon_L. \end{aligned}\tag{63}$$

Observation has that

$$\prod_{i<j}^{L}(\upsilon_i-\upsilon_j) = \det(\upsilon_j^{i-1}). \tag{64}$$

By following the analysis in [56], $\mathbf{D}(x)$ is finally given as

$$\mathbf{D}(x)_{i,j} = \begin{cases}(-1)^{L-K-i}\Gamma(i+j-1), \ \text{for } i \le L-K, \\ \displaystyle\int_0^{+\infty} e^t t^{2L-K-i+j-1}\gamma(L-i+1, \frac{xL}{t})dt, \\ \text{for } i > L-K. \end{cases} \tag{65}$$

To determine the second expression of (65), it is noticed that $\gamma(\cdot,\cdot)$ is defined as [27], [56]

$$\gamma(a,x) = \int_0^x t^{a-1}e^{-t}dt = (a-1)!\left(1 - e^{-x}\sum_{i=0}^{a-1}\frac{x^i}{i!}\right). \tag{66}$$

Furthermore, observation from [59] has that

$$\int_0^{+\infty} x^{\alpha-1}e^{-\beta x-\frac{\gamma}{x}}dx = 2(\frac{\gamma}{\beta})^{\frac{\alpha}{2}}K_\alpha(2\sqrt{\beta\gamma}), \tag{67}$$

where $K_a(b)$ as the modified Bessel function of the first kind. By substituting this (67) and (66) into (65), with tremendous calculation, the determinant expression of its second part can be finally obtained as

$$\begin{aligned}&\int_0^{+\infty} e^t t^{2L-K-i+j-1}\gamma(L-i+1, \frac{xL}{t})dt \\ &= (L-i)!\Bigg[\Gamma(2L-K-i+j) - \sum_{i}^{L-i}\frac{(xL)^i}{i!} \\ &\quad \times 2(xL)^{\frac{2L-K-2i+j}{2}}K_{2L-K-2i+j}(2\sqrt{xL})\Bigg], \ \text{for } i > L-K. \end{aligned}\tag{68}$$

Thus the PDF of $0 < \chi_1 < \ldots < \chi_K < \infty$ can be obtained as

$$f_\chi(x) = \frac{(-1)^{K(L-K)}\frac{d}{dx}[\det(\mathbf{D}(x))]}{\prod_{k=1}^{K}\Gamma(K-k+1)\prod_{i=1}^{L}\Gamma(L-i+1)^2}. \tag{69}$$

In line with [60], the unordered PDF of eigenvalues $\lambda_1,\ldots,\lambda_K$ of $(\mathbf{DBA})(\mathbf{DBA})^H$ conditioned on $\mathbf{BA}$ is

$$\begin{aligned}f_\lambda(\lambda|\mathbf{BA}) = &\frac{1}{L\prod_{i<j}^{K}(\chi_j-\chi_i)} \\ &\times\sum_{m=L-K+1}^{L}\frac{\lambda^{K-L+m-1}}{\Gamma(K-L+m-1)}\det(\mathbf{G}) \end{aligned}\tag{70}$$

whereas $\mathbf{G}$ is a $L \times L$ matrix with entries

$$\mathbf{G}_{i,j} = \begin{cases}\chi_j^{i-1}, & for\ i \ne j \\ \chi_j^{L-K-1}e^{-\frac{\lambda}{\chi_j}}. & for\ i = j. \end{cases} \tag{71}$$

Thus by using $f(\lambda) = f_\lambda(\lambda|\mathbf{BA})f_\chi(x)$ and integrating it to all χ, we can finally obtain the result.

This completes the proof. ■

ACKNOWLEDGMENT

The author would like to thank Prof. Yang Chen with the University of Macau for the valuable discussion and help on the deduction of the relationship between Stieltjes and Shannon transform.

REFERENCES

[1] T. S. Rappaport *et al.*, "Millimeter wave mobile communications for 5G cellular: It will work!" *IEEE Access*, vol. 1, pp. 335–349, May 2013.
[2] F. Rusek *et al.*, "Scaling up MIMO: Opportunities and challenges with very large arrays," *IEEE Signal Process. Mag.*, vol. 30, no. 1, pp. 40–60, Jan. 2013.
[3] R. G. Gallager, *An Inequality Capacity Region Multiaccess Multipath Channels*. New York, NY, USA: Springer, 1994, pp. 129–139.

[4] D. Tse and P. Viswanath, *Fundamentals Wireless Communication*. Cambridge, U.K.: Cambridge Univ. Press, 2005.

[5] Z. Chang *et al.*, "Energy efficient resource allocation for wireless power transfer enabled collaborative mobile clouds," *IEEE J. Sel. Areas Commun.*, vol. 34, no. 12, pp. 3438–3450, Dec. 2016.

[6] Z. Chang, T. Ristaniemi, and Z. Niu, "Radio resource allocation for collaborative OFDMA relay networks with imperfect channel state information," *IEEE Trans. Wireless Commun.*, vol. 13, no. 5, pp. 2824–2835, May 2014.

[7] H. Yang and T. L. Marzetta, "Performance of conjugate and zero-forcing beamforming in large-scale antenna systems," *IEEE J. Sel. Areas Commun.*, vol. 31, no. 2, pp. 172–179, Feb. 2013.

[8] J. Zhang, L. Dai, X. Zhang, E. Björnson, and Z. Wang, "Achievable rate of rician large-scale MIMO channels with transceiver hardware impairments," *IEEE Trans. Veh. Technol.*, vol. 65, no. 10, pp. 8800–8806, Oct. 2016.

[9] L. Dai, X. Gao, X. Su, S. Han, C. L. I, and Z. Wang, "Low-complexity soft-output signal detection based on gauss–seidel method for uplink multiuser large-scale MIMO systems," *IEEE Trans. Veh. Technol.*, vol. 64, no. 10, pp. 4839–4845, Oct. 2015.

[10] L. Dai, Z. Wang, and Z. Yang, "Spectrally efficient time-frequency training OFDM for mobile large-scale MIMO systems," *IEEE J. Sel. Areas Commun.*, vol. 31, no. 2, pp. 251–263, Feb. 2013.

[11] J. G. Andrews, T. Bai, M. N. Kulkarni, A. Alkhateeb, A. K. Gupta, and R. W. Heath, "Modeling and analyzing millimeter wave cellular systems," *IEEE Trans. Commun.*, vol. 65, no. 1, pp. 403–430, Jan. 2017.

[12] Z. Gao, L. Dai, and Z. Wang, "Channel estimation for MmWave massive MIMO based access and backhaul in ultra-dense network," in *Proc. IEEE ICC*, May 2016, pp. 1–6.

[13] Y. Saito, Y. Kishiyama, A. Benjebbour, T. Nakamura, A. Li, and K. Higuchi, "Non-orthogonal multiple access (NOMA) for cellular future radio access," in *Proc. IEEE VTC*, Jun. 2013, pp. 1–5.

[14] J. Choi, "Minimum power multicast beamforming with superposition coding for multiresolution broadcast and application to NOMA systems," *IEEE Trans. Commun.*, vol. 63, no. 3, pp. 791–800, Mar. 2015.

[15] Z. Ding, P. Fan, and H. V. Poor, "Impact of user pairing on 5G nonorthogonal multiple-access downlink transmissions," *IEEE Trans. Veh. Technol.*, vol. 65, no. 8, pp. 6010–6023, Aug. 2016.

[16] Z. Yang, Z. Ding, P. Fan, and Z. Ma, "Outage performance for dynamic power allocation in hybrid non-orthogonal multiple access systems," *IEEE Commun. Lett.*, vol. 20, no. 8, pp. 1695–1698, Aug. 2016.

[17] H. Q. Ngo, E. G. Larsson, and T. L. Marzetta, "Energy and spectral efficiency of very large multiuser MIMO systems," *IEEE Trans. Commun.*, vol. 61, no. 4, pp. 1436–1449, Apr. 2013.

[18] Z. Zhou, M. Dong, K. Ota, R. Shi, Z. Liu, and T. Sato, "Game-theoretic approach to energy-efficient resource allocation in device-to-device underlay communications," *IET Commun.*, vol. 9, no. 3, pp. 375–385, Feb. 2015.

[19] C. Xu *et al.*, "Efficiency resource allocation for device-to-device underlay communication systems: A reverse iterative combinatorial auction based approach," *IEEE J. Sel. Areas Commun.*, vol. 31, no. 9, pp. 348–358, Sep. 2013.

[20] D. Zhang, Z. Zhou, S. Mumtaz, J. Rodriguez, and T. Sato, "One integrated energy efficiency proposal for 5G IoT communications," *IEEE Internet Things J.*, vol. 3, no. 6, pp. 1346–1354, Dec. 2016.

[21] Z. Chang, S. Zhou, T. Ristaniemi, and Z. Niu, "Collaborative mobile clouds: An energy efficient paradigm for content sharing," *IEEE Wireless Commun.*, to be published.

[22] M. R. Akdeniz *et al.*, "Millimeter wave channel modeling and cellular capacity evaluation," *IEEE J. Sel. Areas Commun.*, vol. 32, no. 6, pp. 1164–1179, Jun. 2014.

[23] G. Lee, Y. Sung, and J. Seo, "Randomly-directional beamforming in millimeter-wave multiuser MISO downlink," *IEEE Trans. Wireless Commun.*, vol. 15, no. 2, pp. 1086–1100, Feb. 2016.

[24] A. Alkhateeb, O. El Ayach, G. Leus, and R. W. Heath, Jr., "Channel estimation and hybrid precoding for millimeter wave cellular systems," *IEEE J. Sel. Topics Signal Process.*, vol. 8, no. 5, pp. 831–846, Oct. 2014.

[25] X. Liu and X. Wang, "Efficient antenna selection and user scheduling in 5G massive MIMO-NOMA system," in *Proc. IEEE VTC*, May 2016, pp. 1–5.

[26] Z. Ding and H. V. Poor, "Design of massive-MIMO-NOMA with limited feedback," *IEEE Signal Process. Lett.*, vol. 23, no. 5, pp. 629–633, May 2016.

[27] D. Zhang, K. Yu, Z. Wen, and T. Sato, "Outage probability analysis of NOMA within massive MIMO systems," in *Proc. IEEE VTC*, May 2016, pp. 1–5.

[28] X. Gao, L. Dai, Z. Chen, Z. Wang, and Z. Zhang, "Near-optimal beam selection for beamspace MmWave massive MIMO systems," *IEEE Commun. Lett.*, vol. 20, no. 5, pp. 1054–1057, May 2016.

[29] A. Vinel, Q. Ni, D. Staehle, and A. Turlikov, "Capacity analysis of reservation-based random access for broadband wireless access networks," *IEEE J. Sel. Areas Commun.*, vol. 27, no. 2, pp. 172–181, Feb. 2009.

[30] M. Debbah and R. R. Müller, "MIMO channel modeling and the principle of maximum entropy," *IEEE Trans. Inf. Theory*, vol. 51, no. 5, pp. 1667–1690, May 2005.

[31] R. Couillet, M. Debbah, and J. W. Silverstein, "A deterministic equivalent for the analysis of correlated MIMO multiple access channels," *IEEE Trans. Inf. Theory*, vol. 57, no. 6, pp. 3493–3514, Jun. 2011.

[32] J. Hoydis, S. ten Brink, and M. Debbah, "Massive MIMO in the UL/DL of cellular networks: How many antennas do we need?" *IEEE J. Sel. Areas Commun.*, vol. 31, no. 2, pp. 160–171, Feb. 2013.

[33] A. Lu, X. Gao, and C. Xiao, "A free deterministic equivalent for the capacity of MIMO MAC with distributed antenna sets," in *Proc. IEEE ICC*, Jun. 2015, pp. 1751–1756.

[34] J. Zhang, C.-K. Wen, S. Jin, X. Gao, and K.-K. Wong, "On capacity of large-scale MIMO multiple access channels with distributed sets of correlated antennas," *IEEE J. Sel. Areas Commun.*, vol. 31, no. 2, pp. 133–148, Feb. 2013.

[35] A. Firag, P. J. Smith, and M. R. McKay, "Capacity analysis of MIMO three product channels," in *Proc. AusCTW*, Feb. 2010, pp. 13–18.

[36] Z. Pan, J. Lei, Y. Zhang, X. Sun, and S. Kwong, "Fast motion estimation based on content property for low-complexity H.265/HEVC encoder," *IEEE Trans. Broadcast.*, vol. 62, no. 3, pp. 675–684, Sep. 2016.

[37] J. W. Silverstein and A. M. Tulino, "Theory of large dimensional random matrices for engineers," in *Proc. IEEE 19th Int. Symp. Spread Spectr. Techn. Appl.*, Aug. 2006, pp. 458–464.

[38] Z. Zhou, Y. Wang, Q. M. J. Wu, C. N. Yang, and X. Sun, "Effective and efficient global context verification for image copy detection," *IEEE Trans. Inf. Forensics Security*, vol. 12, no. 1, pp. 48–63, Jan. 2017.

[39] Z. Yang, Z. Ding, P. Fan, and N. Al-Dhahir, "A general power allocation scheme to guarantee quality of service in downlink and uplink NOMA systems," *IEEE Trans. Wireless Commun.*, vol. 15, no. 11, pp. 7244–7257, Nov. 2016.

[40] Y. Liu, Z. Ding, M. Elkashlan, and H. V. Poor, "Cooperative non-orthogonal multiple access with simultaneous wireless information and power transfer," *IEEE J. Sel. Areas Commun.*, vol. 34, no. 4, pp. 938–953, Apr. 2016.

[41] J. Choi, "H-ARQ based non-orthogonal multiple access with successive interference cancellation," in *Proc. IEEE GLOBECOM*, Nov. 2008, pp. 1–5.

[42] Z. Ding, Z. Yang, P. Fan, and H. V. Poor, "On the performance of non-orthogonal multiple access in 5G systems with randomly deployed users," *IEEE Signal Process. Lett.*, vol. 21, no. 12, pp. 1501–1505, Dec. 2014.

[43] T. S. Rappaport, R. W. Heath, Jr., R. C. Daniels, and J. N. Murdock, *Millimeter Wave Wireless Communications*. Westford, MA, USA: Prentice-Hall, 2014.

[44] M. N. Kulkarni, A. Ghosh, and J. G. Andrews, "A comparison of MIMO techniques in downlink millimeter wave cellular networks with hybrid beamforming," *IEEE Trans. Commun.*, vol. 64, no. 5, pp. 1952–1967, May 2016.

[45] H. Zhao *et al.*, "28 GHz millimeter wave cellular communication measurements for reflection and penetration loss in and around buildings in New York city," in *Proc. IEEE ICC*, Jun. 2013, pp. 5163–5167.

[46] S. Collonge, G. Zaharia, and G. E. Zein, "Influence of the human activity on wide-band characteristics of the 60 GHz indoor radio channel," *IEEE Trans. Wireless Commun.*, vol. 3, no. 6, pp. 2396–2406, Nov. 2004.

[47] C.-K. Wen, G. Pan, K.-K. Wong, M. Guo, and J.-C. Chen, "A deterministic equivalent for the analysis of non-Gaussian correlated MIMO multiple access channels," *IEEE Trans. Inf. Theory*, vol. 59, no. 1, pp. 329–352, Jan. 2013.

[48] J. Dehardt, "Generalizations of the Glivenko-Cantelli theorem," *Ann. Math. Statist.*, vol. 42, no. 6, pp. 2050–2055, Dec. 1971.

[49] N. Letzepis and A. Grant, "Shannon transform of certain matrix products," in *Proc. IEEE ISIT*, Jun. 2007, pp. 1646–1650.

[50] J. Gong, S. Zhou, Z. Zhou, and Z. Niu, “Joint optimization of content caching and push in renewable energy powered small cells,” in *Proc. IEEE ICC*, May 2016, pp. 1–6.
[51] C.-K. Wen, S. Jin, and K.-K. Wong, “On the sum-rate of multiuser MIMO uplink channels with jointly-correlated Rician fading,” *IEEE Trans. Commun.*, vol. 59, no. 10, pp. 2883–2895, Oct. 2011.
[52] R. Müller, “On the asymptotic eigenvalue distribution of concatenated vector-valued fading channels,” *IEEE Trans. Inf. Theory*, vol. 48, no. 7, pp. 2086–2091, Jul. 2002.
[53] H. Holma and A. Toskala, *LTE for UMTS: Evolution to LTE-Advanced*, 2nd ed. Hoboken, NJ, USA: Wiley, 2011.
[54] B. M. Hochwald, T. L. Marzetta, and V. Tarokh, “Multiple-antenna channel hardening and its implications for rate feedback and scheduling,” *IEEE Trans. Inf. Theory*, vol. 50, no. 9, pp. 1893–1909, Sep. 2004.
[55] A. M. Tulino and S. Verdú, “Random matrix theory and wireless communications,” *Found. Trends Commun. Inf. Theory*, vol. 1, no. 1, pp. 1–182, 2004.
[56] S. Jin, M. R. McKay, K. K. Wong, and X. Gao, “Transmit beamforming in Rayleigh product MIMO channels: Capacity and performance analysis,” *IEEE Trans. Signal Process.*, vol. 56, no. 10, pp. 5204–5221, Oct. 2008.
[57] H. Zhang, S. Jin, M. R. McKay, X. Zhang, and D. Yang, “High-SNR performance of MIMO multi-channel beamforming in double-scattering channels,” *IEEE Trans. Commun.*, vol. 59, no. 6, pp. 1621–1631, Jun. 2011.
[58] M. Kang and M. S. Alouini, “Impact of correlation on the capacity of MIMO channels,” in *Proc. IEEE ICC*, vol. 4. May 2003, pp. 2623–2627.
[59] D. Zwillinger and V. Moll, *Table of Integrals, Series, and Products*, 8th ed. San Diego, CA, USA: Academic, 2015.
[60] S. Jin, R. McKay, C. Zhong, and K.-K. Wong, “Ergodic capacity analysis of amplify-and-forward MIMO dual-hop systems,” *IEEE Trans. Inf. Theory*, vol. 56, no. 5, pp. 2204–2224, May 2010.

Di Zhang (S’13) received the degree (Hons.) in 2013. He is currently pursuing the Ph.D. degree with Waseda University, Tokyo, Japan. His research interests include massive MIMO, green communications, information theory, and signal processing. He is a Student Member of the IEICE. He served as a TPC member of the IEEE VTC and WCNC workshops in 2016.

Zhenyu Zhou (S’06–M’11) received the M.E. and Ph.D. degrees from Waseda University, Tokyo, Japan, in 2008 and 2011, respectively. From 2012 to 2013, he was the Chief Researcher with the Department of Technology, KDDI, Tokyo. Since 2013, he has been an Associate Professor with the School of Electrical and Electronic Engineering, North China Electric Power University, China. He has also been a Visiting Scholar with the Tsinghua–Hitachi Joint Laboratory on Environment-Harmonious ICT, University of Tsinghua, Beijing, since 2014. His research interests include green communications and smart grid. He is a member of the IEICE and the CSEE. He received the Young Researcher Encouragement Award from the IEEE Vehicular Technology Society in 2009. He served as the Workshop Co-Chair of the IEEE ISADS 2015 and a TPC member of the IEEE VTC 2017, the IEEE VTC 2016, the IEEE ICC 2016, the IEEE ICC 2015, the Globecom 2015, the ACM Mobimedia 2015, and the IEEE Africon 2015.

Chen Xu (S’12–M’15) received the B.S. degree from the Beijing University of Posts and Telecommunications in 2010 and the Ph.D. degree from Peking University in 2015. She is currently a Lecturer with the School of Electrical and Electronic Engineering, North China Electric Power University, China. Her research interests mainly include wireless resource allocation and management, game theory, optimization theory, heterogeneous networks, and smart grid communication. She received the Best Paper Award at the International Conference on Wireless Communications and Signal Processing in 2012 and the IEEE Leonard G. Abraham Prize 2016.

Yan Zhang (M’05–SM’10) received the Ph.D. degree from the School of Electrical and Electronics Engineering, Nanyang Technological University, Singapore. He is currently a Full Professor with the Department of Informatics, University of Oslo, Oslo, Norway. His current research interests include next-generation wireless networks leading to 5G, green and secure cyber-physical systems, such as smart grid, healthcare, and transport. He is an IEEE Vehicular Technology Society (VTS) Distinguished Lecturer. He is also a Senior Member of the IEEE ComSoc, the IEEE CS, the IEEE PES, and the IEEE VTS. He is a fellow of the IET. He is an Associate Technical Editor of the *IEEE Communications Magazine*, an Editor of the IEEE TRANSACTIONS ON GREEN COMMUNICATIONS AND NETWORKING, an Editor of the IEEE COMMUNICATIONS SURVEYS AND TUTORIALS, and an Associate Editor of the IEEE ACCESS. He serves as the Chair in a number of conferences, including the IEEE GLOBECOM 2017, the IEEE PIMRC 2016, the IEEE CloudCom 2016, the IEEE ICCC 2016, the IEEE CCNC 2016, the WCSP 2016, the IEEE SmartGridComm 2015, and the IEEE CloudCom 2015. He serves as a TPC member for numerous international conference, including the IEEE INFOCOM, the IEEE ICC, the IEEE GLOBECOM, and the IEEE WCNC.

Jonathan Rodriguez (M’04–SM’13) received the master’s and Ph.D. degrees in electronic and electrical engineering from the University of Surrey, U.K., in 1998 and 2004, respectively. In 2005, he was a Researcher with the Institutõ de Telecomunicações. He was a Senior Researcher with the Institutõ de Telecomunicações in 2008, where he established the 4TELL Research Group targeting the next generation mobile networks with key interests on energy efficient design, cooperative strategies, security, and electronic circuit design. He has served as a Project Coordinator for major international research projects, such as the Eureka LOOP and the FP7 C2POWER, while acting as the Technical Manager of the FP7 COGEU and the FP7 SALUS. He is currently leading the H2020-ETN SECRET Project, a European Training Network on 5G communications. He joined the University of South Wales, U.K., in 2017, where he was appointed Professor of Mobile Communications. He has authored over 350 scientific works, including nine book editorials. He is a Chartered Engineer (CEng) and Fellow of the IET (FIET) since 2015.

Takuro Sato (F’13) received the Ph.D. degree in electronics engineering from Niigata University, Niigata, Japan, in 1993. Since 1995, he has been a Professor with the Niigata Institute of Technology, where his research focused on CDMA, OFDM, personal communication systems, and other related areas. In 2004, he joined GITS/GITI, Waseda University, Tokyo, as a Professor, where he is currently serving as the Dean. He has been involved in the research on PCM transmission equipment development, mobile communications, data transmission, and digital signal processing. He has developed the wideband CDMA system for personal communication system and joined the PCS Standardization Committee in the USA and Japan. His contributions are mainly in high speed cellular modem standardization for ITU, 2.4GHz PCS for ITA and wireless LAN of the IEEE 802.11. He has authored 11 books and over 200 papers. His current research interests include next generation mobile communications, wireless communications, ICN/CCN technology, ICT in smart grid, and their global standardizations. He is a fellow of the IEICE. He served as the Chair of the IEEE ISADS 2015, the IEEE Globecom 2015, and various other conferences and journal editors.